



# Nanomechanical readout of a single spin

Philipp R. Struck,<sup>\*</sup> Heng Wang, and Guido Burkard

*Department of Physics, University of Konstanz, D-78457 Konstanz, Germany*

(Received 24 October 2013; revised manuscript received 20 December 2013; published 9 January 2014)

The spin of a single electron in a suspended carbon nanotube can be read out by using its coupling to the nanomechanical motion of the nanotube. To show this, we consider a single electron confined within a quantum dot formed by the suspended carbon nanotube. The spin-orbit interaction induces a coupling between the spin and one of the bending modes of the suspended part of the nanotube. We calculate the response of the system to pulsed external driving of the mechanical motion using a Jaynes-Cummings model. To account for resonator damping, we solve a quantum master equation, with parameters comparable to those used in recent experiments, and show how information about the spin state of the system can be acquired by measuring the mechanical motion of the nanotube. The latter can be detected by observing the current through a nearby charge sensor.

DOI: [10.1103/PhysRevB.89.045404](https://doi.org/10.1103/PhysRevB.89.045404)

PACS number(s): 62.25.-g, 63.22.Gh, 85.85.+j, 71.70.Ej

## I. INTRODUCTION

In the past few years, advanced manufacturing techniques have spawned new interest in nanomechanical devices. These are of interest for fundamental research as well as for possible applications. In various experimental setups the cooling of a nanomechanical resonator to its ground state has been achieved [1–3]. It is now possible to study quantum features such as the zero-point motion of objects much larger than the atomic scale [4]. As mechanical motion can be coupled via a wide range of forces, nanomechanical systems have been proposed for various applications such as mass [5,6], force [7], and motion [8] sensing. This versatility also makes hybrid systems of mechanical devices coupled to other systems possible candidates for various applications in quantum information and communications [9]. For example, nanomechanical resonators have been proposed as qubits [10], optical delay lines [11], quantum data buses [12], and quantum routers [13], among others.

One of the challenges in building sensitive nanoelectromechanical systems is to control thermal fluctuations. Only if the device operates at energies significantly higher than the thermal energy can one expect to observe quantum-mechanical behavior in equilibrium. In this context, carbon is a very promising building material because the resulting structures are very light and stiff, which leads to high resonance frequencies. Resonators made of suspended carbon nanotubes (CNTs) are of special interest. They can be produced almost free of defects and with radii on the scale of  $\approx 1$  nm and lengths up to  $1 \mu\text{m}$ , and in addition their bending mode is easily excited. Experimentally, it has been demonstrated that frequencies of more than 4 GHz and quality factors of more than 100 000 are achievable [14,15].

Coupling a localized electron spin to a nanomechanical resonator is of particular interest because such a system may be used as a quantum memory due to the relatively long spin lifetimes [16]. Carbon-based materials, with their weak spin-orbit coupling due to the relatively low atomic mass of carbon and the presence of only a few nuclear spins, are promising

[17]. Recently, the readout of a single spin of the nitrogen-vacancy (NV) center in diamond has been used to read out the oscillatory motion of the magnetized tip of an atomic force microscope [18–21]. However, the well-defined local-field gradient required for this setup is quite challenging. CNTs provide an entirely different arena for the coupling of single spins to nanomechanical resonators, and they can potentially be integrated into scalable (two-dimensional) semiconductor structures.

Here, we propose a method for an all-electrical readout of the state of a single electronic spin. We assume that the spin is confined to an oscillator consisting of a doubly clamped, suspended CNT. While previous experiments [14,15] make use of a charge transport measurement through the CNT, here, we focus on the measurement of the amplitude of the vibrating CNT via a close-by charge sensor, which could be a quantum point contact (QPC) or a quantum dot (QD). Those devices have been shown to be sensitive to charge fluctuations of far less than one elementary charge [22,23]. Very recently, there has been remarkable progress in submicrosecond-time-scale readout of the mechanical motion of a carbon nanotube [24]. The coupling of the spin to the vibrational motion allows the readout of the spin state via measurements of the amplitude of the mechanical vibration [25]. This scheme does not require optical access to the probe or time-dependent magnetic fields, which makes it potentially scalable.

## II. MODEL

The setup under study is shown in Fig. 1. It consists of a CNT suspended over a trench with contacts on both sides and electrostatic gates responsible for the electron confinement. Since the nanotube carries a net charge, a constant (dc) voltage applied to a back gate can be used to tune the mechanical resonance frequency. Furthermore, an ac voltage applied to an external antenna or the back gate can be used to drive the motion of the charged resonator [15,25].

In order to obtain a well-defined qubit, the fourfold degeneracy due to the valley and spin degree of freedom of the CNT has to be lifted (note that for the localized electron, the sublattice degree of freedom is frozen out). A magnetic field  $B$  parallel to the CNT axis in combination with the spin-orbit coupling serves this purpose. Around a field of

<sup>\*</sup>Present address: Continental Reifen Deutschland GmbH, Hannover, Germany.

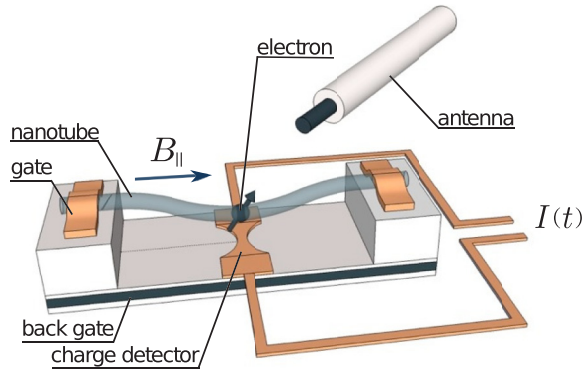


FIG. 1. (Color online) Schematic of the proposed setup of the carbon nanotube (CNT) resonator with a quantum dot containing a single electron. The gates on both sides of the CNT can be electrostatically adjusted to control the number of confined electrons. The back gate is used to tune the resonance frequency of the CNT into resonance with the splitting of the Zeeman sublevels of the electron which make up the qubit. The charge sensor in the vicinity of the vibrating nanotube serves as a detection device for changes in the amplitude due to the coupling of the spin to the vibrational motion. It can be a quantum point contact or a quantum dot which needs to be operated in a regime where the current depends nonlinearly on the gate voltage. A current meter is used to measure a nonlinear current  $I$  which flows through the device.

$B^* \approx \Delta_{SO}/2\mu_B$  two orthogonal spin states within the same valley are split by the Zeeman energy  $\hbar\omega_q = \mu_B(B - B^*)$ . Here,  $\Delta_{SO}$  refers to the intrinsic spin-orbit coupling strength; the intervalley coupling  $\Delta_{KK'}$  is assumed to be much smaller. In the following we assume  $\Delta_{SO} = 370 \mu\text{eV}$  and  $\Delta_{KK'} = 65 \mu\text{eV}$  as realistic parameters [26]. The corresponding states in the opposite valleys are energetically well separated. Thus we can treat the system as an effective two-level system.

For the detection of the nanomechanical oscillation we propose to use the fact that the position  $x(t)$  of the oscillating charged CNT modulates the current through the charge sensor in a (generally) nonlinear way, i.e.,  $I(t) = I_0 + I_1x(t) + I_2x^2(t) + O(x^3)$ . This is the case, for example, when a QD is operated at the maximum of a Coulomb blockade peak. This situation will be assumed for the following discussion. Furthermore, we assume that the frequency  $\omega_p$  of the oscillator is much smaller than the tunneling rate through the charge-sensing device. In this case, at lowest order the charge sensor only probes a time-averaged squared displacement  $\overline{X^2}(\tau) = \frac{1}{\tau} \int_0^\tau dt X^2(t)$ , where  $X^2(t) = \langle x^2(t) \rangle = \text{Tr}[x^2 \rho(t)]$ , with the oscillator density matrix  $\rho$ , and where  $\tau$  is the integration time. In the expansion of  $I(t)$ , only even-order terms in  $x$  appear because  $\overline{x^n} = 0$  for odd  $n$ . Higher-order terms  $n > 2$  are neglected because they contribute only weakly to the current for small displacements  $x(t)$ . Our goal in this paper is to calculate the time-averaged current  $\overline{I}$  through the charge-sensing device as a function of the spin state of the electron.

In the following, we restrict our considerations to one polarization of the bending mode of the CNT. The generalization to two modes is straightforward. When quantized, the resonator displacement  $x$  can be written as  $x = \frac{l_0}{\sqrt{2}}(a + a^\dagger)$ , where  $a$  and  $a^\dagger$  are phonon creation and annihilation operators and  $l_0$  is

the zero-point motion amplitude of the oscillator. In principle there are two ways in which the flexural phonons can couple to the spin. At large phonon energies the usual deformation potential is dominant as it is proportional to  $q^2$ , where  $q$  is the phonon wave number. For lower energies, however, the spin-orbit-mediated deflection coupling  $\propto q$  to flexural phonons dominates [27]. The resulting coupling strength  $g$  will be proportional to both the spin-orbit coupling  $\Delta_{SO}$  and the zero-point amplitude  $l_0$  [28].

As shown earlier [25], the system can be described by the Jaynes-Cummings Hamiltonian

$$H = H_0 + H_d, \quad (1)$$

with

$$H_0 = \frac{\hbar\tilde{\omega}_q}{2}\sigma_z + \hbar g(a\sigma_+ + a^\dagger\sigma_-) + \hbar\tilde{\omega}_p a^\dagger a, \quad (2)$$

$$H_d = \hbar\lambda(a + a^\dagger),$$

where  $\sigma_z$  is a Pauli matrix acting on the spin qubit while  $a$  and  $a^\dagger$  are the creation and annihilation operators for the phonons. The qubit and oscillator frequencies in the rotating frame,  $\tilde{\omega}_q = \omega_q - \omega$  and  $\tilde{\omega}_p = \omega_p - \omega$ , are given as detunings from the driving frequency  $\omega$ . The driving strength  $\lambda$  is assumed to be weak, i.e.,  $\lambda \ll \omega_p$ . In the Jaynes-Cummings model a rotating-wave approximation is incorporated which is valid as long as the driving frequency  $\omega$  is comparable to  $\omega_q$  and  $\omega_p$ .

In addition to the unitary evolution we include the damping of the CNT with a rate  $\Gamma$  which can occur on the same time scale as the readout via the charge detection device. The spontaneous qubit relaxation  $\gamma = 1/T_1$ , where  $T_1$  denotes the spin relaxation time, is neglected because of the very low density of other phonon modes in the vicinity of the bending mode at frequency  $\omega_p$ . Previously, we have shown that with state-of-the-art experimental techniques the strong-coupling regime, i.e.,  $g \gg \Gamma, \gamma$ , is within reach [25]. We neglect the back action on the oscillator caused by the fluctuating charge on the detector [29]. Because the electron tunneling rate  $I/e \sim 100 \text{ GHz}$  (see below) is much larger than the vibration frequency  $\omega_p/2\pi \sim 1 \text{ GHz}$ , the back-action-induced damping and frequency shift are very small [30]. The nonunitary dynamics are described by the quantum master equation for the time evolution of the density matrix  $\rho$ ,

$$\begin{aligned} \dot{\rho} = & -\frac{i}{\hbar}[H, \rho] + (n_B + 1)\Gamma \left( a\rho a^\dagger - \frac{1}{2}\{a^\dagger a, \rho\} \right) \\ & + n_B\Gamma \left( a^\dagger \rho a - \frac{1}{2}\{aa^\dagger, \rho\} \right). \end{aligned} \quad (3)$$

Here,  $n_B = 1/(e^{\hbar\omega_p/k_B T} - 1)$  refers to the Bose-Einstein occupation factor of the phonon bath at temperature  $T$ . The Lindblad terms  $\propto \Gamma$  correspond to emission (absorption) of a phonon to (from) the phonon bath.

While solutions of the quantum master equation (3) cannot be given in closed form, it is worthwhile studying the eigenstates of  $H_0$  first,

$$\begin{aligned} |\psi_{+,n}\rangle &= \cos \frac{\alpha}{2} |\uparrow n - 1\rangle + \sin \frac{\alpha}{2} |\downarrow n\rangle, \\ |\psi_{-,n}\rangle &= -\sin \frac{\alpha}{2} |\uparrow n - 1\rangle + \cos \frac{\alpha}{2} |\downarrow n\rangle \end{aligned} \quad (4)$$

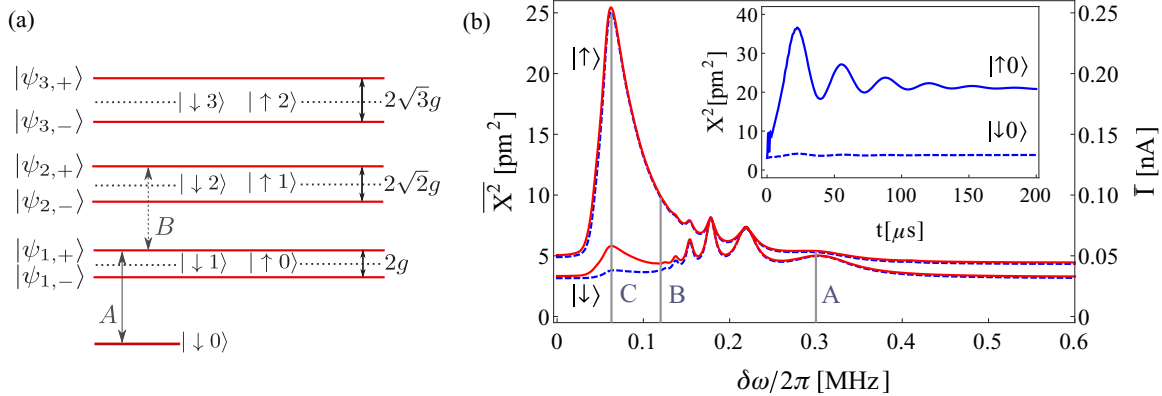


FIG. 2. (Color online) (a) The eigenenergies of  $H_0$  are shown in red. The black dotted lines correspond to the uncoupled, i.e.,  $g = 0$ , case. Note that the ground state is not modified by the coupling  $g$ . The coupling introduces a splitting  $2g\sqrt{n}$ , which is nonlinear in the phonon number  $n$ . (b) The time-averaged squared resonator displacement  $\bar{X}^2(\tau) = \frac{1}{\tau} \int_0^\tau dt X^2(t)$  as a function of the detuning of the driving frequency  $\delta\omega = \omega - \omega_p$  for a fixed integration time of  $\tau = 100 \mu\text{s}$ . Here  $X^2(t) = \langle x^2(t) \rangle = \text{Tr}[x^2 \rho(t)]$ , and  $\rho$  is the oscillator density matrix. The upper (lower) blue dashed line is the evolution at  $T = 0 \text{ mK}$  of the initial state  $|\uparrow 0\rangle$  ( $|\downarrow 0\rangle$ ). The strongest difference between the amplitudes of the two aforementioned initial states is found for a detuning of  $\delta\omega/2\pi = \pm 0.07 \text{ MHz}$  (see mark C). The upper and lower red solid lines correspond to the same initial spin states at a temperature of  $T = 30 \text{ mK}$ . The other parameters are  $\lambda/2\pi = 0.04 \text{ MHz}$ ,  $\omega_p/2\pi = \omega_q/2\pi = 1.5 \text{ GHz}$ ,  $\Gamma = 5 \times 10^4 \text{ Hz}$ , and  $g/2\pi = 0.3 \text{ MHz}$ . At  $30 \text{ mK}$  the thermal energy  $k_B T$  is 2.4 times smaller than  $\hbar\omega_q$ . The label A in both panels (a) and (b) marks the transition from the ground state to the first excited state with positive detuning. The line marked B corresponds to the next transition between states with positive parity. A transition between the states with negative parity requires a negative detuning. In between A and B only two-phonon transitions can occur. The main peak around C at  $\delta\omega \approx 0.07 \text{ MHz}$  is due to several transitions, with the main contribution from the transition between eigenstates  $|\psi_{+,4}\rangle \rightarrow |\psi_{+,5}\rangle$ . This is consistent with the magnitude of the main peak around  $n \sim \bar{X}^2/l_0^2 \sim 4$ . The inset shows the squared amplitude of the CNT as a function of the elapsed time  $t$  for a detuning of the driving frequency of  $\delta\omega/2\pi = 0.07 \text{ MHz}$ . Within the first  $10 \text{ ns}$  the fast Rabi oscillations with the frequency of the coupling strength  $g$  are damped, and following oscillations are caused by the driving strength  $\lambda$ . The resonator reaches a steady state after an interaction time  $1/\Gamma$ .

for  $n \geq 1$  and the special case of the ground state  $n = 0$ :  $|\psi_0\rangle = |\downarrow 0\rangle$ . Here, we use the notation  $|\sigma n\rangle$  for eigenstates of  $H_0$  with  $g = 0$ , i.e.,  $a^\dagger a |\sigma n\rangle = n |\sigma n\rangle$ ,  $\sigma_z |\sigma n\rangle = \sigma |\sigma n\rangle$ , and  $\sigma = \uparrow, \downarrow \equiv \pm 1$ . The mixing angle  $\alpha$  is defined by  $\tan \alpha = \frac{2g\sqrt{n}}{\omega_p - \omega_q}$ . In the resonant case  $\alpha \rightarrow \pi/2$ . The eigenenergies are

$$E_{n,\pm} = \hbar\omega_p \left( n - \frac{1}{2} \right) \pm \hbar\sqrt{\left( \frac{\omega_p - \omega_q}{2} \right)^2 + g^2 n} \quad (5)$$

for  $n \geq 1$  and  $E_0 = -\hbar\frac{\omega_q}{2}$ . For  $n = 0$ , we have  $|\downarrow 0\rangle$  as the ground state. The energy splitting between adjacent eigenstates [see Fig. 2(a)] in the resonant case  $\omega_p = \omega_q$  is  $E_{n+1,\pm} - E_{n,\pm} = \pm[\hbar\omega_p + \hbar g(\sqrt{n+1} - \sqrt{n})]$  and  $E_{n,+} - E_{n,-} = 2\hbar g\sqrt{n}$ .

Since we are interested in the readout of the electron spin, we assume an initial state in which the latter is in one of the two  $\sigma_z$  eigenstates. In the case of  $T = 0$  and an empty QD the oscillator is in its ground state  $|0\rangle$  with the zero-point amplitude  $l_0$ . Directly after loading with an electron, the state of the system is  $|\uparrow 0\rangle$  or  $|\downarrow 0\rangle$ . At temperatures  $T > 0$ , the distribution of phonons obeys Bose-Einstein statistics, and we obtain  $|\Psi(\sigma)\rangle_T = |\sigma\rangle \otimes \frac{1}{Z} \sum_{n=0}^{\infty} e^{-n\hbar\omega_p/k_B T} |n\rangle$  as an initial state, where  $\sigma = \uparrow, \downarrow$  and  $Z = \sum_{n=0}^{\infty} e^{-n\hbar\omega_p/k_B T}$  is the partition function. Experimentally, the state preparation could be performed using techniques that have been established in conventional semiconductor QDs [31]. Raising one of the gates well above the two Zeeman-split qubit levels allows an electron to hop onto the CNT. Provided  $g_{\text{el}}\mu_B B \gg k_B T, g$ , where  $g_{\text{el}}$  is the electron  $g$  factor,  $\mu_B$  is the Bohr magneton,

and  $B$  is the magnetic field, the probability for finding either Zeeman sublevel to be populated is  $1/2$ . A subsequent measurement will then reveal which state was prepared. If the measurement is delayed by a time  $\tau$ , then the population of the higher-energy spin state will decay as  $\sim \exp(-\tau/T_1)$  [22]. To demonstrate the coupling between the spin and phonon and to study the readout this random filling method is sufficient. For possible application in quantum computing, a controlled state preparation is necessary. In this case ferromagnetic leads could be used, as has already been demonstrated for nanotubes deposited on a substrate [32].

### III. RESULTS

We first solve the master equation (3) for the case of  $T = 0$  numerically and calculate the squared oscillator displacement, which is proportional to the current through the charge detection device, in this case a QD. We assume that the oscillator frequency of the fundamental bending mode of the nanotube  $\omega_p/2\pi = 1.5 \text{ GHz}$  is matched by the Zeeman splitting  $\omega_q/2\pi$  of the electron spin (the zero-point motion for this case amounts to  $l_0 = 2.5 \text{ pm}$ ). At this frequency the ground-state energy of the oscillator is 2.4 times smaller than the thermal energy at  $T = 30 \text{ mK}$ . Experimentally, frequencies of suspended nanotubes between  $120 \text{ MHz}$  and  $4.2 \text{ GHz}$  have been reported [14,33]. The coupling strength is chosen to be  $g/2\pi = 0.3 \text{ MHz}$ , which is much larger than the damping of the CNT,  $\Gamma = 0.05 \text{ MHz}$ . Together with the spontaneous relaxation of the qubit  $\gamma$ , which is negligible, the device

can be operated in the strong-coupling regime, i.e.,  $g \gg \Gamma, \gamma$ . The driving strength  $\lambda/2\pi = 0.04$  MHz is chosen to be large enough to compensate for the damping but weak enough not to dominate over the effect of the spin-phonon coupling.

In the inset of Fig. 2(b) the response of the oscillator at temperature  $T = 0$  is plotted as a function of the driving time  $t$  beginning from the initial preparation of the spin state as described above. The driving frequency is detuned from the resonant oscillator and qubit frequencies  $\omega_p = \omega_q$  by  $\delta\omega = \omega - \omega_p$ . The value of  $\delta\omega/2\pi = 0.07$  MHz is found to give the largest difference in amplitude with respect to both initial spin orientations, as we discuss below.

A considerable difference between different initial spin states in the squared amplitude (and therefore in the measured current) can be observed. For the initial state  $|\uparrow 0\rangle$  [see inset of Fig. 2(b)], after the initial fast Rabi oscillations with a frequency  $g$  disappear (on a time scale  $\approx 10$  ns), the dynamics are governed by the slower Rabi oscillations at the frequency of the driving strength  $\lambda$ . The evolution of the initial state  $|\downarrow 0\rangle$  shows only a little effect of the driving. This can be explained by the nonlinearity introduced by the (strong) spin-phonon coupling in the Jaynes-Cummings Hamiltonian (1). When driving with frequencies detuned less than  $(\sqrt{2} - \sqrt{1})g \approx 0.12$  MHz from resonance, the probability to leave the ground state is much less than for all other states.

Typically, the charge detector is too slow to follow the instantaneous motion of the resonator, and it will thus detect an averaged signal  $\bar{I} \propto \bar{X}^2$  caused by the vibrating charge. In the main part of Fig. 2(b) we plot the integrated averaged squared resonator displacement  $\bar{X}^2$  as a function of the detuning of the driving frequency  $\delta\omega$ . As an integration time we choose  $\tau = 100 \mu\text{s}$ ; however, any integration time  $\tau$  of more than  $30 \mu\text{s}$  was found to yield a useful signal.

The peaks can be explained with the help of the spectrum [Fig. 2(a)] of the Jaynes-Cummings Hamiltonian (2). Whenever the driving frequency hits a resonance, energy is absorbed by the oscillator, which results in an increased amplitude. While only positive detunings are shown here, note that the result for negative detunings is exactly the same. The peak at  $\delta\omega/2\pi = 0.3$  MHz  $= g/2\pi$ , denoted by A, for initial state  $|\downarrow 0\rangle$ , for example, is caused by a strong resonant coupling between the ground state  $|\downarrow 0\rangle$  and the dressed state  $|\psi_{+,1}\rangle$ . Note that the smaller peaks between A and B are due to two-phonon processes, which are less pronounced because of the weak driving. The main peak C, centered around 0.07 MHz, is due to transitions between states of equal parity, i.e.,  $|\psi_{+,n}\rangle \rightarrow |\psi_{+,n+1}\rangle$  with  $n \geq 1$ . Line B marks the transitions  $|\psi_{+,1}\rangle \rightarrow |\psi_{+,2}\rangle$ , which corresponds to a detuning of the driving frequency of  $\delta\omega \approx 0.12$  MHz. The main contribution to the large peak C comes from the transition  $|\psi_{+,4}\rangle \rightarrow |\psi_{+,5}\rangle$ , which corresponds to 0.07 MHz. This is consistent with the peak height of  $\bar{X}^2 \approx 25$  pm, which in turn corresponds to a phonon number  $n \sim \bar{X}^2/l_0^2 \sim 4$ . The individual transitions cannot be resolved because the lines are broadened due to the finite damping of the CNT. Note, however, that a finite damping is essential to allow for nonresonant transitions which enable population of higher states. The large energy gap between the ground state and the first excited state due to the nonlinearity

of the spectrum is the reason why the two spin states  $|\uparrow\rangle$  and  $|\downarrow\rangle$  can be resolved.

In Fig. 2(b) the solid red lines show the integrated amplitude in the case of a finite temperature of  $T = 30$  mK. Qualitatively, the same features are observed as for  $T = 0$ , but in this case the integrated amplitude for the initial state  $|\psi(\downarrow)\rangle$  is larger because of the thermal distribution of the oscillator in  $|\psi(\downarrow)\rangle$ , which contains a small admixture of  $|\downarrow 1\rangle$  and higher states in addition to  $|\downarrow 0\rangle$ . We also note that the width of the peak is only a little affected by the finite temperature and is still governed by the damping of the CNT.

To obtain an efficient readout scheme we strive to increase the contrast in the integrated amplitude between spin up and down. A way to achieve this is to change the driving frequency as a function of time. This compensates for the fact that the frequencies of higher transitions are smaller than those of the lower transitions. From Fig. 2(a), we see that the transition frequencies between states of the same parity scale with  $g(\sqrt{n+1} - \sqrt{n})$  (see above). For the sake of simplicity in the following we change the frequency once to demonstrate the principle, but this method could be optimized to further increase the contrast. To achieve the maximum contrast, i.e., the difference between the integrated amplitudes for the two initial states with different spin orientations, we switch the frequency at the point right before the squared amplitude reaches its maximum. The parameters used are the same as in the case of continuous driving. The time at which the driving frequency is switched from 1500.070 to 1500.036 MHz is  $19 \mu\text{s}$ .

The result is shown in Fig. 3(a). We clearly observe an increase in the squared amplitude of the resonator for the case of the initial state  $|\psi(\uparrow)\rangle$ , while the evolution of the other initial state is barely affected. To demonstrate the effectiveness of the driving scheme, we also plot the response of the system when the driving is switched off at  $19 \mu\text{s}$ . As expected, this causes the current to decay exponentially with a rate  $\Gamma$ . This pulsed driving results in lower contrast as long as the integration time  $\tau$  is on the same order as the time scale  $1/\Gamma$  given by the damping and not considerably longer.

In order to discuss the requirements for a spin readout via a measurement of the amplitude of the CNT we use a simple model of a QD tuned to a Coulomb peak in electrical conductance and capacitively coupled to the vibrating charge distribution on the CNT. In the linear regime, i.e., for small source-drain voltage  $V_{\text{sd}}$ , the current is given by  $I(V_1) = V_{\text{sd}}G(V_1)$ . The conductance  $G(V_1)$  is assumed to be a Lorentzian as a function of the gate voltage  $V_1$ , which, due to capacitive coupling of QD and charged CNT, in turn depends on the squared average displacement  $\bar{X}^2$  of the CNT. The average displacement  $\bar{X}$  is zero. To obtain an estimate of the capacitance, we use a simple toy model which consists of three parallel tubes (with the central wire representing the CNT), with pairwise capacitance  $C = \pi\epsilon_0 l / \log[(d + \sqrt{d^2 - 4r^2})/2r]$ , where  $l$  and  $r \ll l$  denote the length and radius of the tubes and  $d \gg l$  is their separation (see the Appendix for further details). Substituting the distance of the displaced tube  $d \pm X$  for  $d$  and expanding both the capacitance and the current  $\bar{I}$  up to second order in  $\bar{X}$  and in the limit of a tube radius much smaller (1 nm) than the distance between

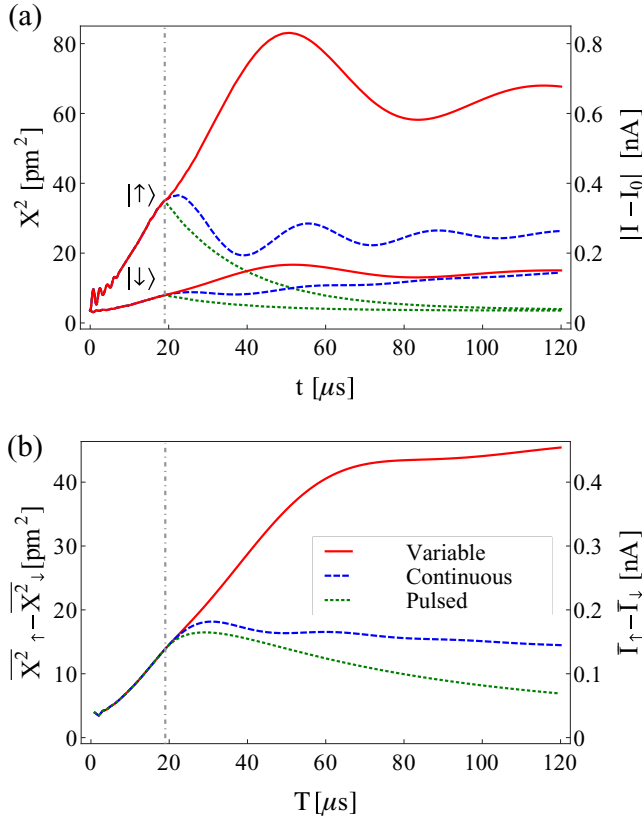


FIG. 3. (Color online) (a) The squared amplitude  $X^2(t) = \langle x^2(t) \rangle = \text{Tr}[x^2 \rho(t)]$  as a function of the elapsed time  $t$  is shown for the cases of continuous (dashed blue line), pulsed (dotted green line), and variable (solid red line) driving. The change of magnitude in the current  $|I_2 X^2(t)| = |I(t) - I_0|$  of spin up and spin down is shown on the right vertical axis. The same parameters as in Fig. 2 are used. The driving frequency  $\omega$  is changed at the time  $t = 19 \mu\text{s}$  right before the amplitude is largest. (b) The difference of the time-averaged squared amplitudes between spin up and spin down  $\overline{X^2}(\tau)_{\uparrow} - \overline{X^2}(\tau)_{\downarrow}$ , on the left vertical axis. The three curves show the integrated signal for the same driving modes as in (a). On the right vertical axis we indicate the difference of the corresponding time-averaged squared current through the QD,  $\overline{I}(\tau)_{\uparrow} - \overline{I}(\tau)_{\downarrow}$ . The current is integrated over an interval  $[0, \tau]$  given by the integration time  $\tau$ . The variable driving scheme results in an increase in current signal by a factor of about 2.

the CNT and the QD ( $d_{12} \simeq 50$  nm), we obtain

$$\begin{aligned} \overline{I(X)} &= I_0 + I_2 \overline{X^2} \\ &= V_{\text{sd}} G_0 \left( 1 - \frac{e^2}{\pi^2 \Delta V^2 \epsilon_0^2 l^2 d^2} \overline{X^2} \right), \end{aligned} \quad (6)$$

where  $G_0$  is the maximum conductance,  $G_0 = 2e^2/h$ , and  $\epsilon_0$  is the vacuum permittivity. For the width of the Coulomb peak of the charge sensor, we assume  $\Delta V = 0.1$  mV [34],  $V_{\text{sd}} = 250$  μV [22], and  $l \simeq 50$  nm. With these values we find a constant background current  $I_0 \approx 20$  nA. The change in current for a maximum squared amplitude of 83 pm [cf. Fig. 3(a)] is  $I_2 \overline{X^2} \approx -0.83$  nA, which corresponds to a fluctuation in the current of about 4.2%. An alternative

mechanical readout method would make use of a second suspended and nearby CNT, acting as a charge sensor. In Fig. 3(b), we show both the integrated difference in average squared amplitude and the corresponding current for the two different initial states for the three kinds of driving.

#### IV. CONCLUSION

In conclusion, we have theoretically shown how the spin state of an electron coupled to a nanomechanical resonator can be read out through an adjacent charge sensor. Here, we have studied the case where the charge sensor is a quantum dot, but similar considerations hold for the case of a quantum point contact, with a slightly altered value of  $I_2$ . The readout scheme is all electrical and requires no optical access to the device or any magnetic field gradients, which is promising in view of its potential for scaling to many qubits. We presented a numerical study of the readout using realistic experimental parameters. We use a simplified model of the QD and the system geometry to demonstrate that with currently available experimental techniques spin readout via the mechanical motion should be possible. For small detuning of the driving frequency we observe a maximum contrast between initial states with spin up and spin down. The contrast decreases with increasing temperature but is still significant at dilution refrigerator temperatures. We have also shown that more elaborate driving schemes in which the driving frequency is a function of time can lead to a large increase in contrast. Additional refinements may be used to further increase the amplitude of the resonator and thus the sensitivity and speed of the spin readout.

#### ACKNOWLEDGMENTS

We thank Andras Palyi for fruitful discussions. This work was supported by the DFG under the programs FOR 912 and SFB 767.

#### APPENDIX: CHARGE READOUT

Here, we describe our simple model used to estimate the sensitivity of the detection of the CNT motion via a nearby charge sensor. The model consists of three capacitively coupled tubes (Fig. 4), where the center tube (2) represents the CNT while the other two represent the charge-sensor gate electrode (1) and a ground plane (3). We assume that the CNT is grounded ( $V_2 = 0$ ), while the ground plane can be voltage biased (later, we will set  $V_3 = 0$  as well). The voltage  $V_1$  on the sensor electrode then influences the transport through the QD, which is tuned such that in the absence of any displacement of the CNT ( $x = 0$ ), the QD is at a Coulomb blockade peak with conductance  $G_0 = 2e^2/h$ . The conductance around the Coulomb blockade peak will have Lorentzian shape,

$$\begin{aligned} \frac{G}{G_0} &= \frac{1}{1 + [V_1(X) - V_1(0)]^2 / \Delta V^2} \\ &\approx 1 - \left( \frac{V_1(X) - V_1(0)}{\Delta V} \right)^2, \end{aligned} \quad (A1)$$

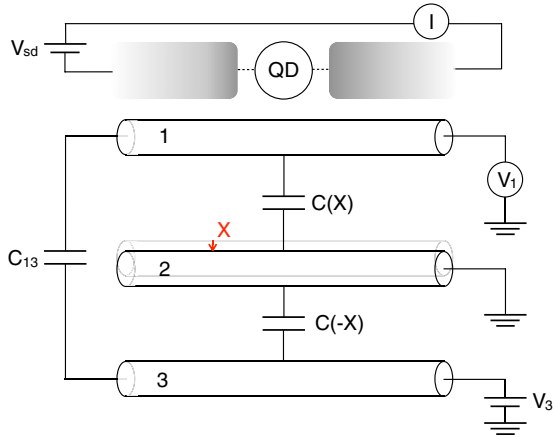


FIG. 4. (Color online) Capacitor model for the charge readout of the motional degree of freedom of a CNT. The CNT (2), ground plane (3), and charge-sensor gate (1) are modeled as cylinders of length  $l$ . The distance between (1) and (2) [(2) and (3)] is  $d + X$  ( $d - X$ ), where  $X$  denotes the vibrational displacement of the CNT. The corresponding capacitances are denoted  $C(X)$  and  $C(-X)$ . The electrostatic potential of the CNT (2) is set to zero (ground). If the potential of (3) is also fixed at a voltage  $V_3$  (e.g.,  $V_3 = 0$ ), then the motion of the CNT (2) by an amount  $X$  leads to an extra charge on the gate (1), which is manifested as in the voltage  $V_1$ . The charge-sensor gate voltage  $V_1$  can then be used to bias the current  $I$  through a QD with voltage bias  $V_{sd}$ .

where we have assumed that the QD stays close to the Coulomb blockade peak. The width of the Coulomb peak is given by  $\Delta V$ . We now use a simple capacitor model to calculate  $V_1(X)$ . The charges on the three conductors are denoted

$Q_1$ ,  $Q_2 = q$ , and  $Q_3$  and are related to the voltages via the capacitance matrix,

$$\begin{pmatrix} Q_1 \\ q \\ Q_3 \end{pmatrix} = \begin{pmatrix} C(X)+C_{13} & -C(X) & -C_{13} \\ -C(X) & C(X)+C(-X) & -C(-X) \\ -C_{13} & -C(-X) & C(-X)+C_{13} \end{pmatrix} \begin{pmatrix} V_1 \\ 0 \\ V_3 \end{pmatrix}, \quad (\text{A2})$$

where  $C_{13}$  denotes the direct capacitance between conductors 1 and 3, and the conductances between conductors 2 and 1 (3) depend on the displacement  $X$  via  $C(X)$  [ $C(-X)$ ]. The capacitance between two parallel tubes of radius  $r$ , length  $l \gg r$ , and distance  $d \gg r$  in vacuum ( $\epsilon = 1$ ) is given by

$$C(0) = \frac{\pi \epsilon_0 l}{\log\left(\frac{d+\sqrt{d^2-4r^2}}{2r}\right)} \approx \frac{\pi \epsilon_0 l}{\log(d/r)}. \quad (\text{A3})$$

For the displaced CNT, we replace  $d$  by  $d + X$  and obtain the capacitance

$$C(X) = \frac{\pi \epsilon_0 l}{\log[(d+X)/r]} \approx C(0) \left(1 - \frac{X}{d \log(d/r)}\right), \quad (\text{A4})$$

where we have used  $X \ll d$ .

For the gate voltage, we find

$$V_1(X) = -\frac{q + V_3 C(-X)}{C(X)}, \quad (\text{A5})$$

and thus, for  $V_3 = 0$ ,

$$[V_1(X) - V_1(0)]^2 = -\frac{q^2}{\pi^2 \epsilon_0^2 d^2 l^2} X^2. \quad (\text{A6})$$

Substituting this into Eq. (A1), using  $I = G V_{sd}$ , and taking the temporal average directly yield Eq. (6).

- 
- [1] A. D. O'Connell, M. Hofheinz, M. Ansmann, R. C. Bialczak, M. Lenander, E. Lucero, M. Neeley, D. Sank, H. Wang, M. Weides *et al.*, *Nature (London)* **464**, 697 (2010).
  - [2] J. Chan, T. P. M. Alegre, A. H. Safavi-Naeini, J. T. Hill, A. Krause, S. Groblacher, M. Aspelmeyer, and O. Painter, *Nature (London)* **478**, 89 (2011).
  - [3] J. D. Teufel, T. Donner, D. Li, J. W. Harlow, M. S. Allman, K. Cicak, A. J. Sirois, J. D. Whittaker, K. W. Lehnert, and R. W. Simmonds, *Nature (London)* **475**, 359 (2011).
  - [4] A. H. Safavi-Naeini, J. Chan, J. T. Hill, Thiago P. Mayer Alegre, A. Krause, and O. Painter, *Phys. Rev. Lett.* **108**, 033602 (2012).
  - [5] H. J. Mamin and D. Rugar, *Appl. Phys. Lett.* **79**, 3358 (2001).
  - [6] H. B. Peng, C. W. Chang, S. Aloni, T. D. Yuzvinsky, and A. Zettl, *Phys. Rev. Lett.* **97**, 087203 (2006).
  - [7] K. Jensen, K. Kim, and A. Zettl, *Nat. Nanotechnol.* **3**, 533 (2008).
  - [8] J. D. Teufel, T. Donner, M. A. Castellanos-Beltran, J. W. Harlow, and K. W. Lehnert, *Nat. Nanotechnol.* **4**, 820 (2009).
  - [9] P. Treutlein, C. Genes, K. Hammerer, M. Poggio, and P. Rabl, *arXiv:1210.4151*.
  - [10] V. Fiore, Y. Yang, M. C. Kuzyk, R. Barbour, L. Tian, and H. Wang, *Phys. Rev. Lett.* **107**, 133601 (2011).
  - [11] A. H. Safavi-Naeini, T. P. M. Alegre, J. Chan, M. Eichenfield, M. Winger, Q. Lin, J. T. Hill, D. E. Chang, and O. Painter, *Nature (London)* **472**, 69 (2011).
  - [12] P. Rabl, S. J. Kolkowitz, F. H. L. Koppens, J. G. E. Harris, P. Zoller, and M. D. Lukin, *Nat. Phys.* **6**, 602 (2010).
  - [13] S. J. M. Habraken, K. Stannigel, M. D. Lukin, P. Zoller, and P. Rabl, *New J. Phys.* **14**, 115004 (2012).
  - [14] A. K. Hüttel, G. A. Steele, B. Witkamp, M. Poot, L. P. Kouwenhoven, and H. S. J. van der Zant, *Nano Lett.* **9**, 2547 (2009).
  - [15] G. A. Steele, A. K. Hüttel, B. Witkamp, M. Poot, H. B. Meerwaldt, L. P. Kouwenhoven, and H. S. J. van der Zant, *Science* **325**, 1103 (2009).
  - [16] D. Loss and D. P. DiVincenzo, *Phys. Rev. A* **57**, 120 (1998).
  - [17] B. Trauzettel, D. V. Bulaev, D. Loss, and G. Burkard, *Nat. Phys.* **3**, 192 (2007).
  - [18] S. Kolkowitz, A. C. Bleszynski Jayich, Q. P. Unterreithmeier, S. D. Bennett, P. Rabl, J. G. E. Harris, and M. D. Lukin, *Science* **335**, 1603 (2012).
  - [19] P. Rabl, P. Cappellaro, M. V. Gurudev Dutt, L. Jiang, J. R. Maze, and M. D. Lukin, *Phys. Rev. B* **79**, 041302 (2009).

- [20] G. Balasubramanian, I. Y. Chan, R. Kolesov, M. Al-Hmoud, J. Tisler, C. Shin, C. Kim, A. Wojcik, P. R. Hemmer, A. Krueger *et al.*, *Nature (London)* **455**, 648 (2008).
- [21] S. D. Bennett, S. Kolkowitz, Q. P. Unterreithmeier, P. Rabl, A. C. B. Jayich, J. G. E. Harris, and M. D. Lukin, *New J. Phys.* **14**, 125004 (2012).
- [22] J. M. Elzerman, R. Hanson, J. S. Greidanus, L. H. Willems van Beveren, S. De Franceschi, L. M. K. Vandersypen, S. Tarucha, and L. P. Kouwenhoven, *Phys. Rev. B* **67**, 161308 (2003).
- [23] L. M. K. Vandersypen, J. M. Elzerman, R. N. Schouten, L. H. Willems van Beveren, R. Hanson, and L. P. Kouwenhoven, *Appl. Phys. Lett.* **85**, 4394 (2004).
- [24] H. B. Meerwaldt, S. R. Johnston, H. S. J. van der Zant, and G. A. Steele, *Appl. Phys. Lett.* **103**, 053121 (2013).
- [25] A. Pályi, P. R. Struck, M. Rudner, K. Flensberg, and G. Burkard, *Phys. Rev. Lett.* **108**, 206811 (2012).
- [26] F. Kuemmeth, S. Ilani, D. C. Ralph, and P. L. McEuen, *Nature (London)* **452**, 448 (2008).
- [27] M. S. Rudner and E. I. Rashba, *Phys. Rev. B* **81**, 125426 (2010).
- [28] See Supplemental Material to Ref. [25].
- [29] A. A. Clerk and S. Bennett, *New J. Phys.* **7**, 238 (2005).
- [30] D. A. Rodrigues, A. D. Armour, *New J. Phys.* **7**, 251 (2005).
- [31] R. Hanson, B. Witkamp, L. M. K. Vandersypen, L. H. Willems van Beveren, J. M. Elzerman, and L. P. Kouwenhoven, *Phys. Rev. Lett.* **91**, 196802 (2003).
- [32] S. Sahoo, T. Kontos, J. Furer, C. Hoffmann, M. Gräber, A. Cottet, and C. Schönenberger, *Nat. Phys.* **1**, 99 (2005).
- [33] J. Chaste, M. Sledzinska, M. Zdrojek, J. Moser, and A. Bachtold, *Appl. Phys. Lett.* **99**, 213502 (2011).
- [34] C. W. J. Beenakker, *Phys. Rev. B* **44**, 1646 (1991).